Journal of Dental Sciences 19 (2024) 479—491

Available online at www.sciencedirect.com

ScienceDirect

journal homepage: www.e-jds.com

Original Article

Biofabricated poly (γ-glutamic acid) bio-ink reinforced with calcium silicate exhibiting superior mechanical properties and biocompatibility for bone regeneration

Ming-Hui Chien [a†], Cheng-Yu Chen [b†], Chun-Liang Yeh [a], Hsin-Yi Huang [c], Han-Yi Chou [d], Yi-Wen Chen [e,f], Chun-Pin Lin [a,g,h*]

[a] *Graduate Institute of Clinical Dentistry, School of Dentistry, National Taiwan University, Taipei, Taiwan*
[b] *x-Dimension Center for Medical Research and Translation, China Medical University Hospital, Taichung, Taiwan*
[c] *Graduate Institute of Dental Science and Oral Health Industries, China Medical University, Taichung, Taiwan*
[d] *Graduate Institute of Oral Biology, School of Dentistry, National Taiwan University, Taipei, Taiwan*
[e] *Graduate Institute of Biomedical Sciences, China Medical University, Taichung, Taiwan*
[f] *Department of Bioinformatics and Medical Engineering, Asia University, Taichung, Taiwan*
[g] *Department of Dentistry, National Taiwan University Hospital, Taipei, Taiwan*
[h] *School of Dentistry, College of Dental Medicine, Kaohsiung Medical University, Kaohsiung, Taiwan*

Received 24 August 2023; Final revision received 4 September 2023
Available online 20 September 2023

KEYWORDS
3D hydrogel;
γ-glutamic acid;
Calcium silicate;
Bone regeneration;
Light curing

Abstract *Background/purpose:* The modification in 3D hydrogels, tissue engineering, and biomaterials science has enabled us to fabricate novel substitutes for bone regeneration. This study aimed to combine different biomaterials by 3D technique to fabricate a promising all-rounded hydrogel for bone regeneration.
Materials and methods: In this study, glycidyl methacrylate (GMA)-modified poly γ-glutamic acid (γ-PGA-GMA) hydrogels with calcium silicate (CS) hydrogel of different concentrations were fabricated by a 3D printing technique, and their biocompatibility and capability in bone regeneration were also evaluated.
Results: The results showed that CS γ-PGA-GMA could be successfully fabricated, and the presence of CS enhanced the rheological and mechanical properties of γ-PGA-GMA hydrogels, thus

* Corresponding author. Graduate Institute of Clinical Dentistry, School of Dentistry, National Taiwan University, No. 1, Chang-Te Street, Taipei 10048, Taiwan.
E-mail address: chunpinlin@gmail.com (C.-P. Lin).
† The two authors had equal contribution to this work.

https://doi.org/10.1016/j.jds.2023.09.008
1991-7902/© 2023 Association for Dental Sciences of the Republic of China. Publishing services by Elsevier B.V. This is an open access article under the CC BY-NC-ND license (http://creativecommons.org/licenses/by-nc-nd/4.0/).

making them more adept at 3D printing and implantations. SEM images of the surface structure showed that higher CS concentrations (5% and 10%) contributed to denser surface architectures, thus achieving improved cellular adhesion and stem cell proliferation. Furthermore, higher concentrations of CS resulted in elevated expressions of osteogenic-related markers such as alkaline phosphatase (ALP) and osteocalcin (OC), as well as enhanced calcium deposition represented by the increased Alizarin Red S staining. In vivo studies referring to critical defects of rabbit femur further showed that the existence of hydrogels alone was able to induce partial bone regeneration, demonstrated by the results from quantitative and qualitative analysis of micro-CT scans. However, CS alterations caused significant increases in bone regeneration, as indicated by micro-CT and histological staining.

Conclusion: These results robustly suggest combining different biomaterials is crucial to producing a well-rounded hydrogel for tissue regeneration. We hope this study could be applied as a platform for others to brainstorm potential out-of-the-box solutions, contributing to developing high-potential biomaterials for bone regeneration.

© 2023 Association for Dental Sciences of the Republic of China. Publishing services by Elsevier B.V. This is an open access article under the CC BY-NC-ND license (http://creativecommons.org/licenses/by-nc-nd/4.0/).

Introduction

The incidence of bone defects increases in line with the population's age caused by trauma, inflammation, or tumor resection remains a significant challenge in clinical treatment.[1] Bioactive materials have been demonstrated as the most significant key in tissue engineering for bone regeneration, playing an effective role in the activation and mineralization of osteoblast cells. The ideal bone substitute should be biodegradable and non-cytotoxic with low immunogenicity and able to provide a suitable microenvironment for cell migration, differentiation, and proliferation.[2] There currently circulate a number of bone regeneration materials on the market, covering calcium silicate (CS), calcium phosphate, sodium sulfate, and bioglass, which are widely applied in bone regeneration applications, of which CS is the most popular biomaterial for clinical bone regeneration with its high biocompatibility, mechanical properties, and osteoinductive capabilities.[3–5] Recently, several studies reported an advanced preparation technique allowing us to fabricate CS nano-particles with mesopores, thus serving as a carrier for controlled drug release.[6–8] Therefore, it is necessary to develop a biomaterial that can be easily delivered to the damaged site and effectively promote long-term tissue regeneration.

Hydrogel is an excellent bridging tool in tissue engineering with its favorable biocompatibility, degradability, and tailorable mechanical properties.[9–11] Previous studies have demonstrated that hydrogels based on collagen, polysaccharide, or gelatin could mimic the native microenvironment, thus enhancing cellular viability, proliferation, and differentiation in comparison with bioceramics hydrogels.[12,13] This is possible since the polymers mentioned above were similar in structure as compared to native extracellular matrices (ECM).[14] Hydrogels have been widely used in tissue engineering as a drug delivery platform for long-term cartilage regeneration, wound healing, and angiogenesis studies.[15,16] Most importantly, growth factors and drugs could be loaded into the hydrogels, contributing to consistent local delivery of factors during hydrogel degradation. Considering this, specific target molecules can be loaded into the three-dimensional hydrogel to activate specific osteogenic signaling pathways to enhance osteogenic-related gene and protein expressions. As a single-chain polyamine acid, the γ-glutamic acid hydrogels (γ-PGA) are derived from native peptides with similar structures as ECM.[17] Similar to the other hydrogels, γ-PGA was reported to possess excellent biocompatibility, non-cytotoxic, and tailorable biodegradability, with good encapsulation characteristics. In addition, γ-PGA was also regarded as a suitable candidate for a drug carrier platform, with high anti-bacterial and anti-dermatitis capacity due to its high water absorption and retention capability. Liu et al. further developed boron-cross linked glycidyl methacrylate (GMA)-modified poly γ-glutamic acid (γ-PGA-GMA) with DL-1,4-dithiothreitol hydrogels and demonstrated that the hydrogels exhibited a mechanical strength of 0.9 MPa which could enhance rabbit's bone marrow stem cell attachment, proliferation, and subsequent cartilage regeneration.[18] From the studies above, it could be speculated that hydrogels could be further modified to enhance bioactivity and regenerative capabilities for soft tissue engineering. However, the mechanical strength of the hydrogels still remained insufficient for hard tissue engineering, such as bone tissue engineering.[19]

In order to modify the mechanical properties of the hydrogels, a photo-initiator could be added to contribute to the formation of cross-linking bonds, serving by absorbing an appropriate wavelength of light and decomposing into free radicals to initiate photopolymerization and forming bonds within the hydrogels.[20] In recent years, the modification of light-curing technology has significantly promoted the progression of hydrogel for drug delivery applications.[21] Various common natural and polymer materials involving gelatin, silk fibroin, and chitosan were modified with photopolymerizable components to produce hydrogels with enriched mechanical properties.[22–24] The porosity, swelling rate, encapsulation capabilities, and degradation rate of the hydrogel can be further adjusted with different light-curing parameters. Amongst the photo-initiators, the Lithium Phenyl(2,4,6-trimethyl benzoyl)phosphinate (LAP) has been developed, which was reported to be biocompatible and has a lower dose required to achieve

polymerization.[25] Photo-polymerizable hydrogels have since been applied in numerous fields of tissue engineering, covering cartilage, bone, heart, and dental regeneration.[26] Hou et al. reported a method combining photo-polymerizable gelatin methacrylate (GelMA) modified with hydroxyapatite to develop a hydrogel with excellent mechanical properties, porosity, and bioactivity for bone regeneration.[27]

In this study, we encapsulated calcium silicate (CS) by γ-PGA-GMA hydrogel and fabricated 3D hydrogel by light-curing processing. The physical and chemical properties of γ-PGA-GMA hydrogel with CS were evaluated according to gelation timing, micromorphology, phase structure, functional group, degree of grafting, stretch/stress loading properties, and degradation rates. In addition, the compatibility of CS/γ-PGA-GMA hydrogel was assessed with human umbilical mesenchymal stem cells (HUMSC) by PrestoBlue and Live/Dead assay. Furthermore, alkaline phosphate (ALP) assay and Alizarin Red staining were applied to evaluate in vitro cell differentiation and mineralization capabilities. Lastly, the CS/γ-PGA-GMA hydrogels were implanted into critical femoral defects of rabbit models, whose regenerative capabilities were further evaluated depending on micro-CT and immunohistochemical staining. This study serves as a novel platform for future drug delivery studies by displaying the possibilities of combining various suitable biomaterials and the application of photo-curing technologies.

Materials and methods

γ-PGA-GMA hydrogel synthesis

γ-PGA-GMA was prepared according to our previously published methods.[22] First, 40 g of γ-PGA powder (average molecular weight 1250 kDa, Vedan, Taichung, Taiwan) was added to 400 mL of deionized water and stirred at 50 °C to obtain a 10% γ-PGA solution. Next, 19.2 mL of glycidyl methacrylate (GMA, Sigma-Aldrich, St. Louis, MO, USA) was added to the solution and stirred at 60 °C for 30 min. The mixture was then centrifuged at 8000 rpm and 40 °C for 30 min. Subsequently, the supernatant was collected and placed into a dialysis bag (10K MWCO, Thermo Fisher Scientific, Waltham, MA, USA) for 6 h of dialysis. The γ-PGA-GMA was collected and lyophilized for 24 h, then stored for further usage. Prior to usage, the γ-PGA-GMA was sterilized with UV light for 30 min. The number and type of chemical functional groups in the molecule were determined via NMR analysis. The γ-PGA-GMA samples were ground into powder and fully dissolved in 0.5 mL D_2O. 1^H NMR characterization was performed by an amx-500 nuclear magnetic resonance instrument of Bruker Company, Germany, with a temperature of 25 °C.

Synthesis of calcium silicate (CS)

Calcium silicate (CS) powder was prepared according to methods published previously,[28] normally composed of calcium oxide (CaO, Sigma-Aldrich, St. Louis, MO, USA), silicon dioxide (SiO_2, Sigma-Aldrich, St. Louis, MO, USA), and aluminum oxide (Al_2O_3, Sigma-Aldrich, St. Louis, MO, USA), which were evenly mixed and stirred, placed in a sintering furnace and sintered at 1400 °C for 2 h. The sintered compound was then cooled for 2 h to room temperature. The CS bulk was mixed with anhydrous alcohol, centrifuged, and ground using a planetary ball mill for 12 h to obtain the micro-grade powder, which was then stored in a dry environment until further usage.

Preparation of light-curing CS/γ-PGA-GMA hydrogel

Firstly, 0.25% lithium phenyl-2,4,6-trimethyl benzoyl phosphonate (LAP, Sigma-Aldrich, St. Louis, MO, USA) was dissolved in phosphate-buffered saline (PBS, Invitrogen, Grand Island, NY, USA) and filtered through a 0.22 μm sieve to remove unwanted products. Then, 10% γ-PGA-GMA combined with different proportions of calcium silicate (0, 2, 5, and 10 wt%) was added to the dissolved LAP to obtain γ-PGA-GMA solutions, which were then stored in a dark, sterile polymerizable cabinet for further usage. Finally, the γ-PGA-GMA solution was injected into the cylinder mold (diameter:10 mm, height:10 mm) and irradiated with UV light for 90 s to prepare γ-PGA-GMA hydrogel.

Characterization of the γ-PGA-GMA hydrogel

The surface phase structure of hydrogel and X-ray diffraction (XRD) patterns were obtained through an X-ray diffractometer (Bruker D8 SSS, Karlsruhe, Germany) at a 5°/min rate in the scanning range of 20—50°. To determine the chemical structure of the deposited minerals, the attenuated total reflection Fourier transformed infrared spectroscopy (FTIR, Vertex 80v, Bruker, Germany) spectrometer in the range of 500—4000 cm^{-1} with a resolution of 4 cm^{-1}. The surface morphology of the nanofibers and films was characterized with a scanning electron microscope (SEM, JSM-7001F, JEOL, Tokyo, Japan). The rheology was followed by the manufacturer's manual. The frequency sweep experiment was performed in parallel plate mode in a Modular Compact Rheometer, Anton Paar, under isothermal conditions with force of 1 N, in an angular frequency range of 0.1—10 rad/s at a constant shear strain of 0.05%. The sample weight and the gap between the two parallel plates are maintained constant at 0.5 g and 1 mm, respectively. To estimate the mechanical properties of different nanofiber hydrogels, we conducted uniaxial tensile testing with a universal mechanical testing machine (Instron 5567, Canton, MA, USA), where each sample ($n = 5$) was cut into rectangular shapes (length: 30 mm, width: 10 mm, thickness: 0.1 mm) before testing. The stress-strain curves were obtained at a rate of 0.5 mm/min. The Young's modulus, ultimate tensile strength, and the elongation at break were calculated according to stress-strain curves.

In vitro soaking

The simulated body fluid (SBF) solution applied in this study had compounds similar to human blood plasma, composed of 7.9949 g of NaCl, 0.2235 g of KCl, 0.147 g of K_2HPO_4, 0.3528 g of $NaHCO_3$, 0.071 g of Na_2SO_4, 0.2775 g of $CaCl_2$, and 0.305 g of $MgCl_2$ in $6H_2O$, in 1000 mL of distilled H_2O.

The pH was adjusted to 7.4 with hydrochloric acid and tris (hydroxymethyl) aminomethane. After immersion for differential durations, the hydrogels were removed from SBF and weighed on a laboratory scale (TE214S, Sartorius, Goettingen, Germany) to acquire the in vitro degradation profile. In addition, inductively coupled plasma atomic emission spectroscopy (ICP-AES, PerkinElmer OPT 1 MA 3000DV, Shelton, CT, USA) was adopted to measure the amount of released Si ion after periods times of immersion. Six hydrogels were examined for each test, with the average recorded.

Cell culture

This study involved the 3rd to 8th generation of human umbilical mesenchymal stem cells (HUMSC, ScienCell Research Laboratories, Carlsbad, CA, USA). The HUMSC were cultured with a commercial medium (#4651, ScienCell Research Laboratories, Carlsbad, CA, USA) with 500 mL basal medium, 25 mL fetal bovine serum, 5 mL growth supplement, and 5 mL penicillin/streptomycin solution. The HUMSC were then cultured in a 37 °C incubator with 5% CO_2 with the culture medium replaced every two days.

Cell proliferation and viability

After 1, 3, and 7 days of culture, PrestoBlue® reagent (PrestoBlue™ Cell Viability Reagent, Invitrogen, Grand Island, NY, USA) was added to the culture dishes and left to react for 4 h. Then, 100 μL of the solution was pipetted into a fresh 96-well plate for absorbance analysis with a spectrophotometer (Infinite Pro M200, Tecan, Männedorf, Switzerland) at 570 nm wavelength taking a reference wavelength of 650 nm. For the viability test, the hydrogels were removed from the culture medium, rinsed with PBS, and treated with live/dead viability/cytotoxicity kits (Invitrogen, Grand Island, NY, USA). The cell viability was observed under a confocal microscope (Leica TCS SP8, Wetzlar, Germany). The images of the live and dead cells were marked with green and red fluorescence, respectively.

Alizarin red S staining

After 7 and 14 days of culture in hydrogels with an osteogenic differentiation medium, accumulated calcium deposition on the HUMSC was analyzed using alizarin red S staining. Firstly, the specimens were fixed and stained with alizarin red S solution (pH = 4) for 20 min. After this, the hydrogels were washed several times and photographed under a BX53 Olympus fluorescence microscope (Olympus, Tokyo, Japan) at 200× magnification. In addition, the absorbance of the alizarin red S stain was quantified using a spectrophotometer at 450 nm. All experiments were performed in triplicate.

Establishment of the critical-sized bone defect model

The in vivo experimental protocol was approved by the Animal Experimental Ethics Committee of China Medical University in Taichung, Taiwan (CMUIACUC-2019-099-1). New Zealand white male rabbits aged 3 months and weighing 1.8—2.0 kg were purchased from the National Laboratory Animal Center (Taipei, Taiwan), and critically sized defects of the distal femoral epiphysis (6 mm in diameter, 6 mm in depth) were induced in them. The rabbits were divided into three groups of three rabbits each. The rabbits in the two groups were implanted with CS0 and CS10, respectively, which was not conducted in the other group. The rabbits were first anesthetized with chlorhexidine by injection and then anesthetized continuously with 100% oxygen with a gas anesthesia machine (Engler ADS1000) containing 5% isoflurane. Before the skin was dissected with a scalpel, the hair on the hind legs was shaved with an electric shaver and disinfected with alcohol and iodine. The muscle fascia was then dissected to expose the femur, avoiding dissecting excess muscle and basic structures, such as nerves and blood vessels. The hydrogel was implanted into the defect site, and the wound was closed with sutures and covered with a thick mask of anti-inflammatory ointment. All rabbits fasted for 1 day before surgery.

Micro-computed tomography (μ-CT) and histological staining

After 28 days, the samples were retrieved in accordance with protocols approved by our ethical committee, then washed, fixed, and sectioned at 6 mm a piece (OCT®) (KMA-0100-00A, CellPath Ltd., Newtown, Wales, UK). Afterward, a microtome was taken to prepare 6 μm sections from each specimen. The sections were then stained with hematoxylin and eosin (HE, ScyTek Lab., West Logan, UT, USA), a modified Masson's trichrome stain kit (MT, ScyTek Lab., West Logan, UT, USA), and a von Kossa kit (VK, ScyTek Lab., West Logan, UT, USA), where Trichrome staining in blue was applied to identify collagen, Von Kossa staining in red to observe the difference between the osteoid tissue and the calcified bone. A BX53 Olympus microscope was used for the examination of the samples.

Statistical analyses

A one-way statistical analysis of variance (ANOVA) was applied to analyze the significance of the between-group differences in each experiment. Scheffe's multiple comparison test was carried out to determine the significant deviations of each sample. The statistical solutions were defined so that a P-value <0.05 could be considered statistically significant, as indicated by an *.

Results

Characterization of γ-PGA-GMA

A schematic diagram summarizing the preparation of γ-PGA-GMA hydrogels and the transformations in chemical structures post-modifications were depicted in Fig. 1 γ-PGA-GMA hydrogel was synthesized through the ring-opening reaction of γ-PGA hydrogel and GMA. Due to its

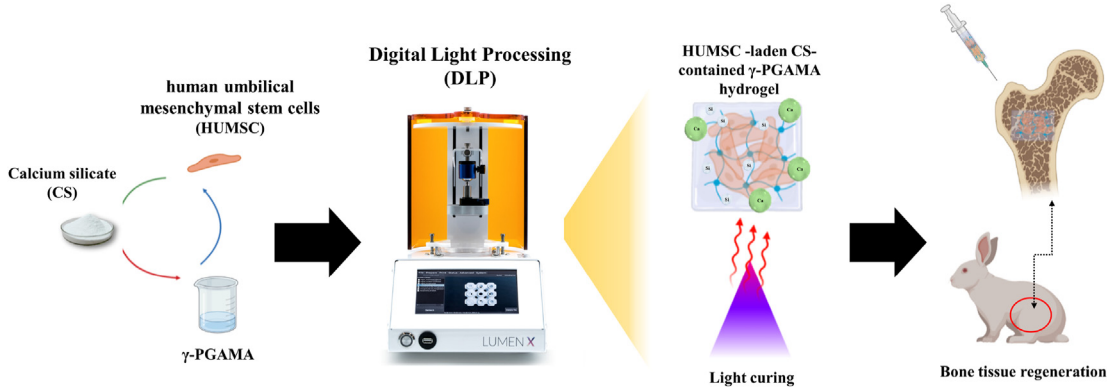

Figure 1 Schematic for the digital light processing (DLP) fabrication and function of γ-PGA-GMA/CS hydrogels for bone regeneration. (γ-PGA, poly γ-glutamic acid; GMA, glycidyl methacrylate; CS, calcium silicate).

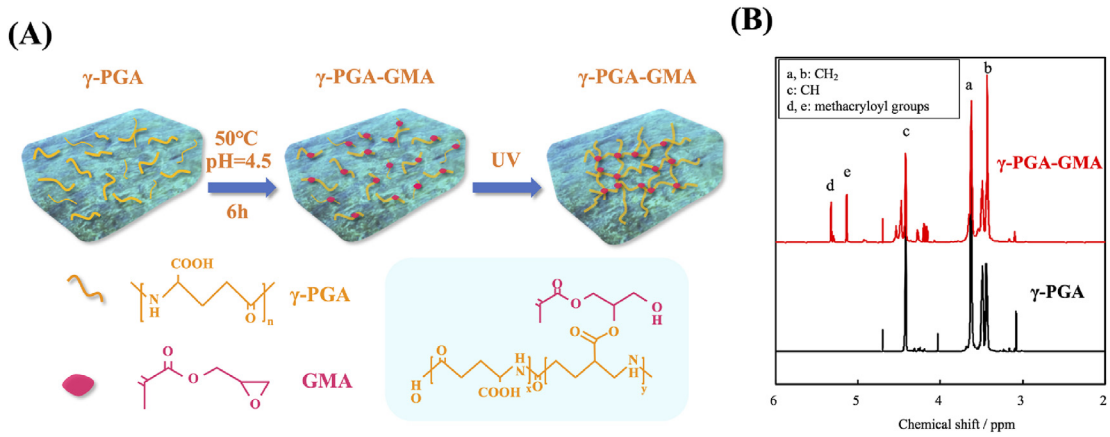

Figure 2 (A) Synthesis of γ-PGA hydrogel into γ-PGA-GMA, (B) NMR analysis for ^{1}H NMR spectrum of γ-PGA hydrogel with GMA.

weak mechanical properties, LAP, a photo-initiator cross-linking under 350 nm UV exposure, was incorporated for photo-curability for tailoring and modifying its mechanical properties. Adding a photo-initiator also enables us to fabricate hydrogels of various shapes and sizes, referring to the area of defect due to post-printing modifications with UV exposures. In addition, CS, a biomaterial widely used in bone regeneration, was added to elevate its osteo-capabilities, considering its osteoinduction characteristics. NMR was conducted to examine the successful incorporation of γ-PGA-GMA, as shown in Fig. 2.

The physicochemical properties of CS/γ-PGA-GMA hydrogel

Fig. 3 exhibited the differences in outlook between γ-PGA-GMA hydrogels with different concentrations of CS, where all hydrogels were fabricated via molding technique. γ-PGA-GMA was combined with different concentrations of CS with labels as follows: CS0 (0% CS), CS2 (2% CS), CS5 (5% CS), and CS10 (10% CS). The hydrogels were designed to be 10 mm × 10 mm × 5 mm in size. CS0 was transparent in color, gradually becoming milky white with the increase in CS concentrations. CS2 appeared translucent, while CS5 and CS10 appeared homogenous and milky compared to the rest. These indicate that the color variations of the hydrogels were directly related to the concentrations of CS in the hydrogels, and the addition of CS was expected to enhance hydrogel mechanical strength to promote bone regeneration. Overall, the hydrogels have the capacity to retain the elastic characteristics of γ-PGA-GMA, developing better mechanical strength with increasing CS concentrations. The

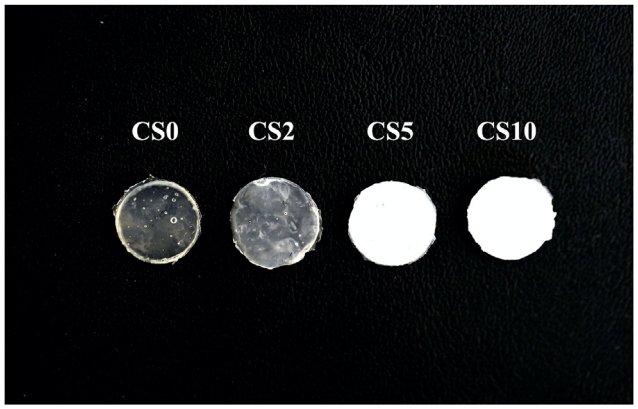

Figure 3 The morphology of γ-PGA-GMA/CS hydrogel with different calcium silicate (CS) concentrations. (CS0 = 0% CS; CS2 = 2% CS; CS5 = 5% CS; CS10 = 10% CS).

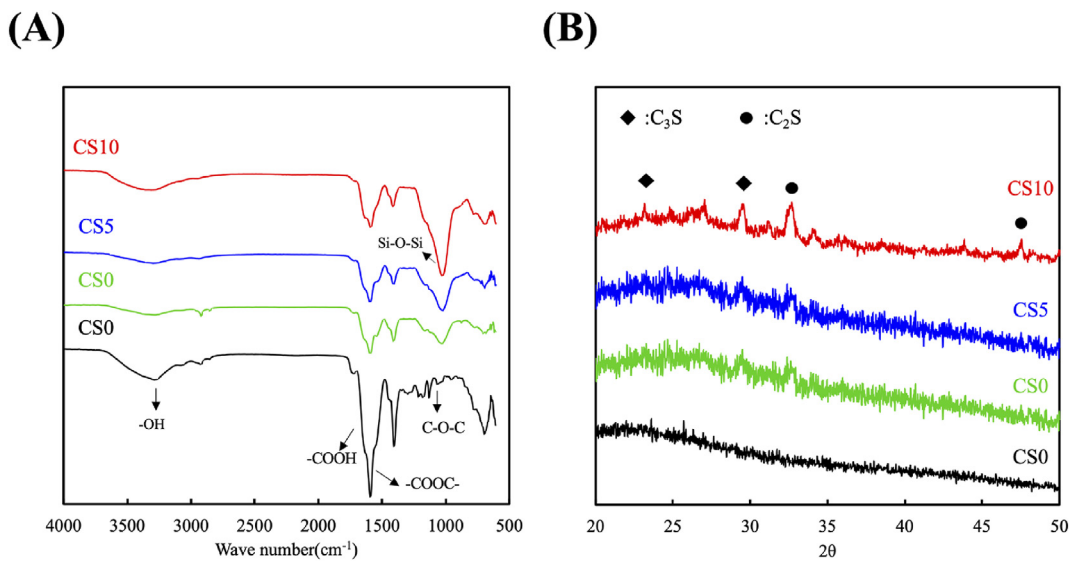

Figure 4 (A)The functional group of FTIR and (B) phase structure of XRD results for the different concentrations of calcium silicate (CS) contained γ-PGA-GMA hydrogel.

capability of CS in promoting bone regeneration was evaluated and described in the results below.

FTIR analysis was conducted further to confirm the incorporation of CS into our γ-PGA-GMA hydrogels, as shown in Fig. 4A. The interphase patterns of the various materials were identified by XRD analysis as an essential tool further to confirm the successful modification of CS into γ-PGA-GMA. As seen in Fig. 4B, CS0 had the typical crystalline peaks of γ-PGA at 2θ of 23.2°, 29.6°, and 32.5°. In addition, the CS-modified hydrogels notably exhibited the presence of CS peaks with increasing intensity at 2θ in the range of 29°—34°. The results showed that CS was successfully added to γ-PGA-GMA while retaining the structural characteristics of γ-PGA.

Rheological analysis of the various hydrogels was evaluated, as shown in Fig. 5A. The sol-gel temperature of a hydrogel is critical for effective extrusion and printing, where the gelation temperature of G' and G" was determined to be 25.0 °C. Despite the addition of CS, all groups reported a sol-gel curing duration of approximately 80 s, with CS5 and CS10 exhibiting a higher storage modulus in comparison with CS2 and CS0, suggesting the robust coexistence of CS with γ-PGA-GMA and LAP photoinitiators. In addition, the mechanical properties of the hydrogels were evaluated and presented in the form of a stress-strain curve (Fig. 5B). The mechanical properties of a hydrogel are a crucial feature deserving consideration as sufficient mechanical strength is required for the hydrogels to withstand the harsh native environment after implantation for supporting regeneration. In addition, enhanced mechanical properties allowed for easier and better handling during surgical procedures. The results

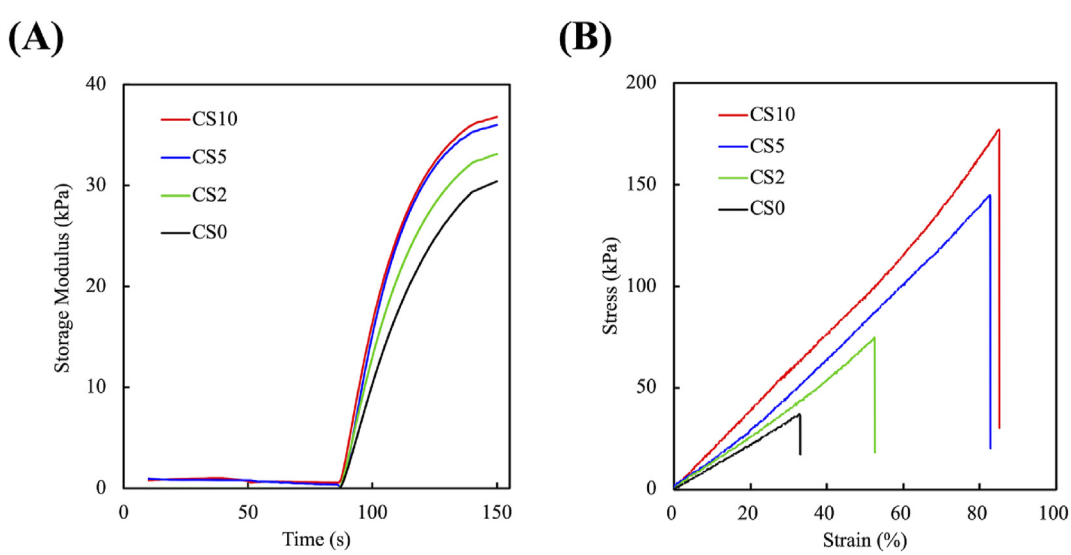

Figure 5 The evolution of (A) dynamic rheology properties and (B) stress-strain curve for CS0, CS2, CS5, and CS10 hydrogel. Data presented as mean ± SEM, n = 6 for each group. (SEM, standard error of mean).

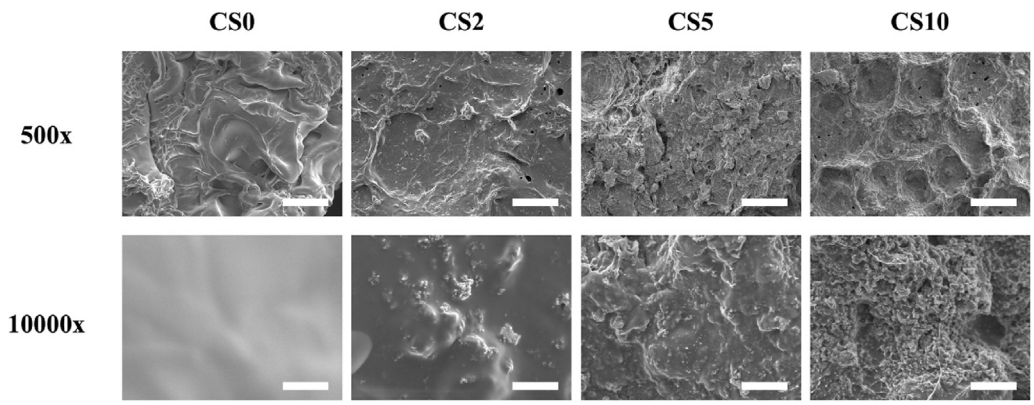

Figure 6 Surface microstructure of γ-PGA-GMA/CS hydrogel with different calcium silicate (CS) concentrations. The scale bar is 1 μm.

indicated a direct relation of the mechanical properties with the concentrations of CS with CS10, exhibiting more than 5x enhanced mechanical strength compared to CS0. In addition, CS0, CS2, CS5, and CS10 were able to withstand 37.4 ± 3.9, 74.8 ± 5.1, 144.9 ± 8.3, and 177.2 ± 10.1 kPa with 33.1%, 52.6%, 82.8% and 85.2% strain, respectively. As the results above indicated, it was further speculated that the increased mechanical properties benefit from the presence of additional chemical bonds between CS and γ-PGA-GMA.

Microstructure of CS/γ-PGA-GMA hydrogel

To investigate the relationship between CS, surface architecture, as well as their effects on cellular behavior, surface structures of fabricated hydrogels were analyzed using the scanning electron microscope in Fig. 6. The CS0 retained a smooth and flat surface without obvious depositions, while the other three groups of hydrogels displayed a more rough and rugged texture with depositions on the surfaces with increasing concentrations of CS. Thus, we can conclude that these surface topographical transformations attributed to the addition of CS are directly related to its concentrations.

Weight loss

The degradation rates of the CS/γ-PGA-GMA were determined by assessing pre-and post-immersion weights of the hydrogels, as shown in Fig. 7A. The degradation rates of the CS-contained γ-PGA-GMA varied between groups, where CS0 showed the highest degradation rate for all time points. Rapid degradation was displayed in all groups during the 2 weeks of immersion before slowing down to a gradual degradation rate till 4 weeks of immersion. CS0, 2, 5, and 10 were noted to exhibit a weight loss of 67.6 ± 5.0%, 59.8 ± 3.1%, 50.2 ± 3.7%, and 40.6 ± 3.8% after 4 weeks of soaking. Degradation rates in vivo are a significant factor in determining the ideal biomaterials for tissue regeneration,[29] which are supposed to ideally match the regeneration rates of tissues to provide ample structural support and nutrient transport.

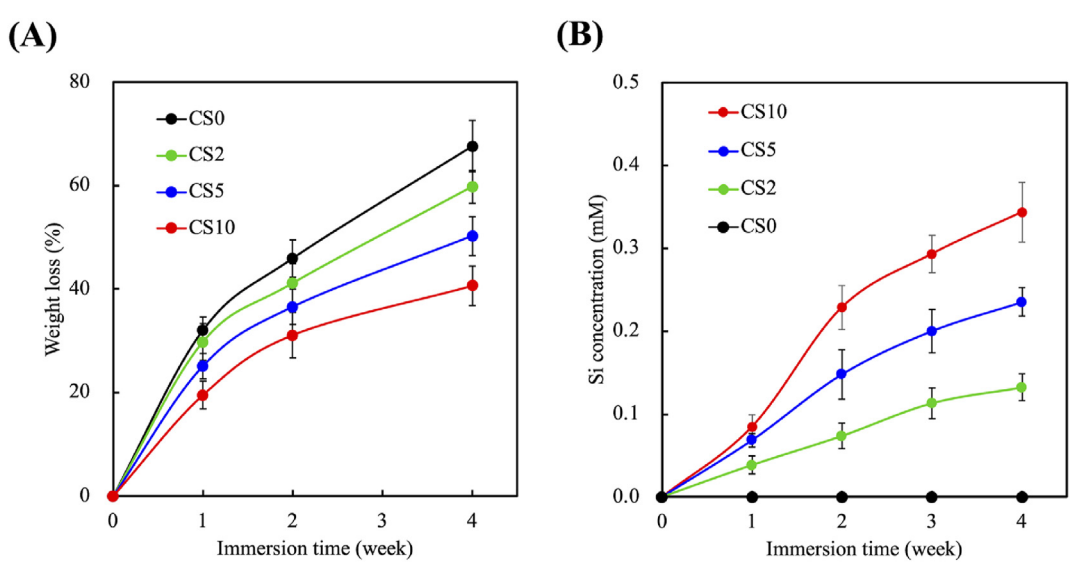

Figure 7 The (A) degradation and (B) Si ion released properties of γ-PGA-GMA/CS hydrogels with different calcium silicate (CS) concentrations soaked in SBF for 1 month. Data presented as mean ± SEM, n = 6 for each group.

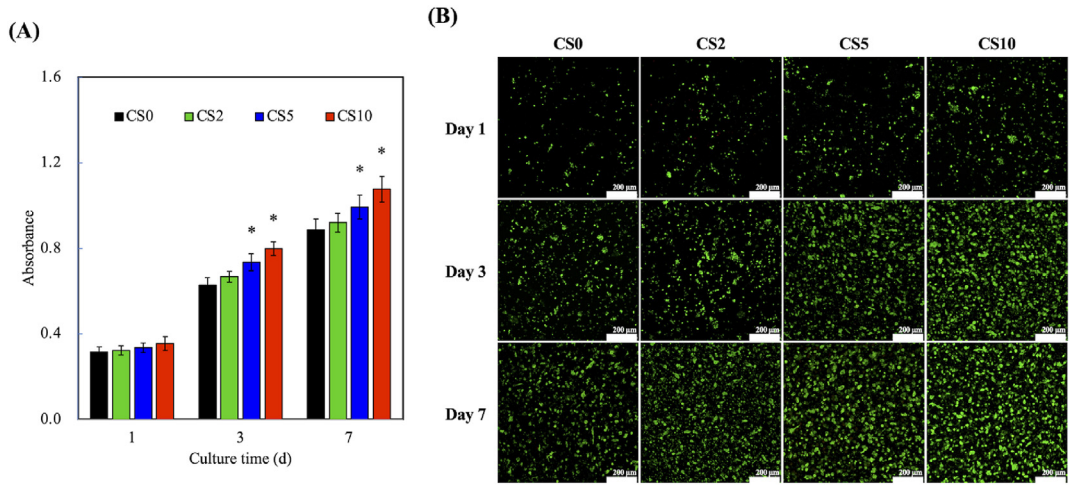

Figure 8 (A) The proliferation of the HUMSC cultured in γ-PGA-GMA/CS hydrogel for 1, 3, and 7 days. * indicates a significant difference ($P < 0.05$) when compared to CS0. (B) The cytoskeleton for F-actin filament (green) staining of HUMSC cultured in γ-PGA-GMA/CS hydrogel for 1, 3, and 7 days. The scale bar of the photograph is 100 μm. (HUMSC, human umbilical mesenchymal stem cells).

The levels of Si ion released during 4 weeks of immersion were recorded, as shown in Fig. 7B. CS10 showed a gradual increase in Si release during the 2 weeks of soaking, with the levels of Si ion from the CS10 hydrogels after 2 and 4 weeks of immersion to be 0.29 ± 0.02 and 0.34 ± 0.04 mM while from CS2 be 0.11 ± 0.02 and 0.13 ± 0.02 mM, respectively.

Cell proliferation and morphology in HUMSC-laden γ-PGA-GMA hydrogels

HUMSC cultured in the CS/γ-PGA-GMA hydrogels for 7 days were evaluated for proliferation and immunofluorescence, as shown in Fig. 8. As seen from the quantification results, no significant differences were noted in all groups after 1 day of culture. However, CS5 and CS10 exhibited significantly higher levels of proliferation from day 3 onwards as compared to CS0. The increased cellular proliferation was speculated to be promoted by the levels of released CS from CS/γ-PGA-GMA hydrogels. Furthermore, elevated surface roughness and modified mechanical properties of the hydrogels also acted as contributing factors to the increased cellular proliferation of the CS/γ-PGA-GMA hydrogels. As the immunofluorescence results in Fig. 8B depicted, more cells in the CS5 and CS10 groups appeared on days 3 and 7 of culture compared to CS0. In addition, cellular adhesion could be consulted to estimate the hydrophilic properties of the hydrogels indirectly. Consistently, the hydrophilic capability of the CS/γ-PGA-GMA hydrogels was not affected by the addition of CS as the cells well adhered after 1 day of a culture characterized by their spindle-like shapes and flat appearances. This morphology is consistent with results reported by others that encapsulated cells in hydrogels with adequate cell attachment motifs, such as RGD sequences, which appeared flattered and spindled, which would then cause cells to be spherical and cluster if lacking.

Furthermore, even after 7 days of culture, more than 80% of the cells were still noted to be well adhered to the surfaces of the hydrogels, indicating the favorability of the micro-environment of the hydrogels, which is conducive to cellular activity. The cell viability and metabolic activity in this study could be explained by the cross-linking densities and degradation profiles of each hydrogel. Increased cross-linking densities and slower degradation rates of CS10 provide ample and stable contact angles for cells to adhere and attach to. However, it is worth noting that slow degradation could reduce cellular viability to a large extent due to the entrapment of cells, limited nutrient provision, and waste removal. Also, the above results proved that CS/γ-PGA-GMA hydrogels and their degraded by-products were non-cytotoxic.

Osteogenesis-related protein expression

In order to compare and analyze the effects of CS concentrations in promoting bone regeneration, several osteogenesis-related markers involving ALP and OC were evaluated, as shown in Fig. 9. ALP expression level was evaluated to be the highest in CS10, followed by CS5 and CS2, with the lowest observed in CS0 (Fig. 9). The difference was especially evident on day 7 of culture, whereby CS10 displayed 1.6-fold higher expression levels as compared to CS0. The activity of ALP was strengthened in line with concentrations of CS. Similarly, the expression levels of OC were also directly proportional to the concentrations of CS, with the highest OC levels observed in CS10. On day 7 of culture, the expression levels of OC were 2.1-fold higher in CS10 as compared to that in CS0.

Mineralization

The levels of bone regeneration were evaluated with Alizarin Red S staining, as shown in Fig. 10, which was applied to detect calcium mineral deposition. Calcium mineral

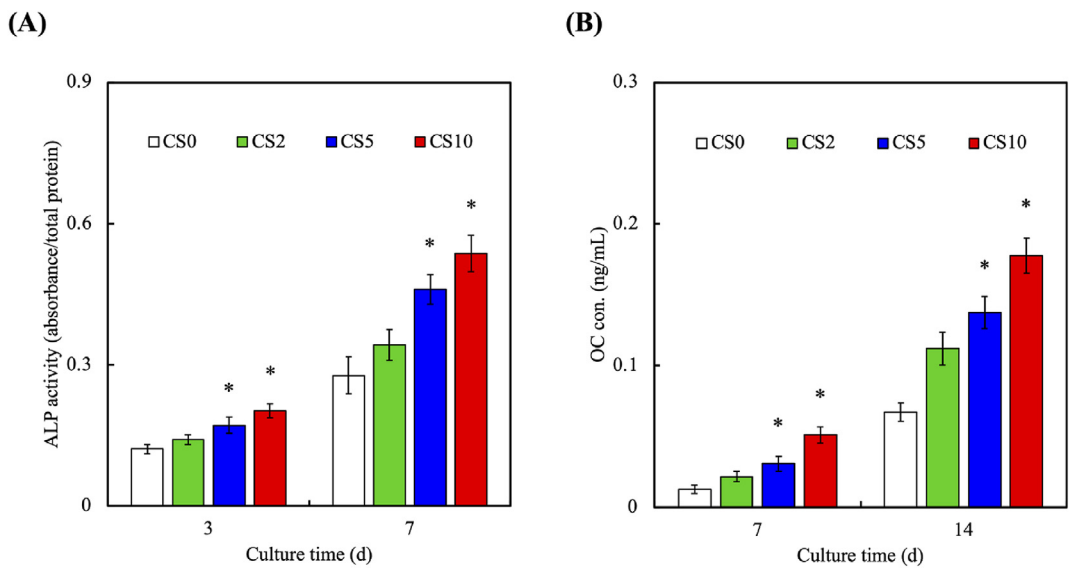

Figure 9 Osteogenesis in early and late stages markers of (A) ALP activity and (B) OC expression of HUMSC cultured in γ-PGA-GMA/CS hydrogel for different time points. * indicates a significant difference ($P < 0.05$) from CS0. Data presented as mean ± SEM, n = 6 for each group. (ALP, alkaline phosphatase; OC, osteocalcin).

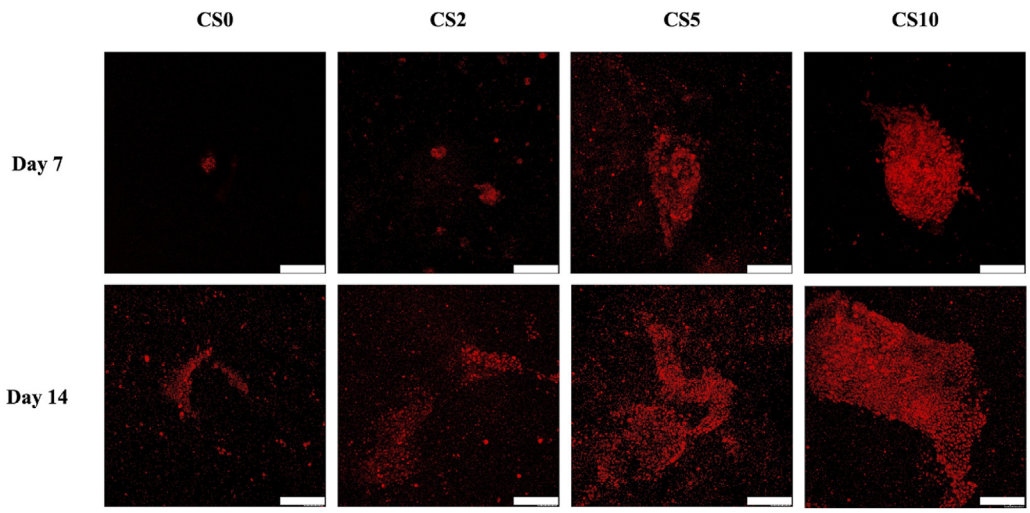

Figure 10 Alizarin Red S staining of HUMSC to assess calcium mineral deposits after being cultured in γ-PGA-GMA/CS hydrogel for 7 and 14 days. The scale bar is 200 μm.

deposition was reported in all groups after 7 and 14 days of culture, where CS10, nevertheless, had the highest calcium mineral deposition and nodule formation as compared to the other groups at all time points, which reached a good agreement with the expression levels of osteogenic-related markers above.

In vivo bone regeneration

To further assess the in vivo osteogenesis of the prepared CS/γ-PGA-GMA, the hydrogels were implanted into the femur defects of rabbits. After 4 weeks of implantation, new bone formation was evaluated by conducting qualitative and quantitative micro-CT, as shown in Fig. 11. The reduced surface area of bone defects indicated that the presence of hydrogels alone could induce partial bone regeneration compared to control (Ctl, defect only). However, the defects filled with CS10 hydrogels were almost regenerated and healed after 4 weeks of implantation. Further bone volume and trabecular thickness quantification were carried out, as shown in Fig. 11B and C. CS10 had the highest BV/TV ratio of 38.5%, followed by CS0 at 19.0% and Ctl at 4%. The results of Tb.Th measurements reporting the highest trabecular thickness observed in CS10 were consistent with the findings above. The differences between the results of CS10 and Ctl were demonstrated to be statistically significant ($P < 0.05$). Therefore, the results robustly suggest that the presence of hydrogels was capable of promoting bone regeneration and that our novel hydrogels, with the addition of CS were able to modify bone regeneration and bone thickness to a large

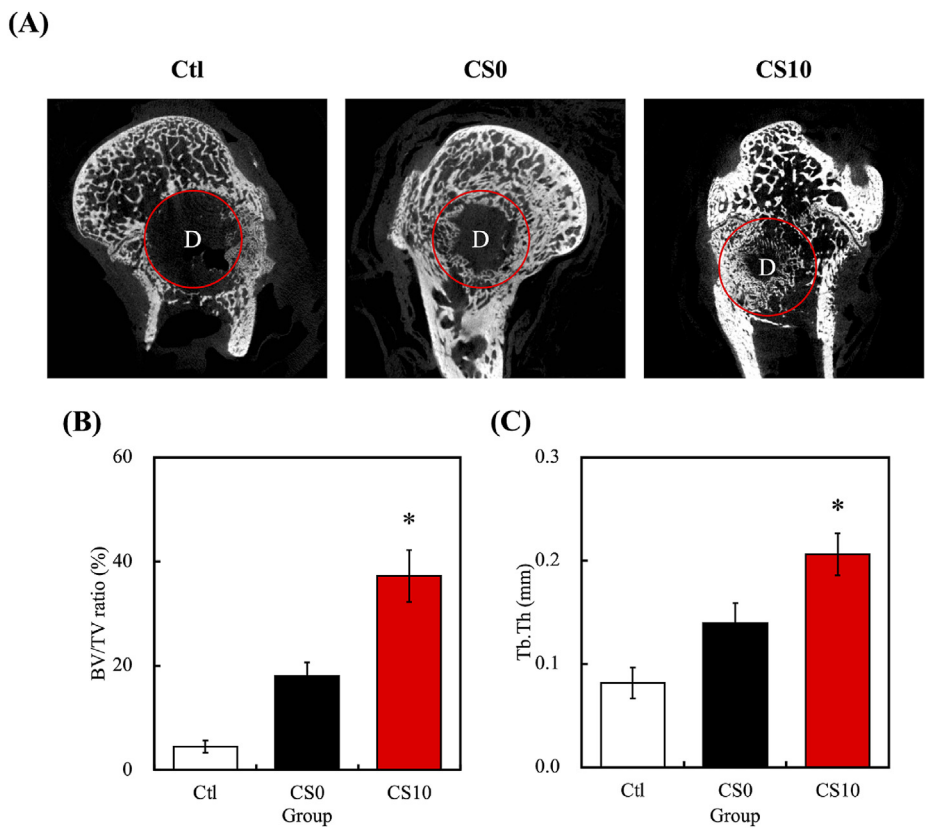

Figure 11 Micro-CT analysis showing the morphology of bone regeneration. (A) Neo bone ingrowth defects site after it underwent 8-week regeneration with hydrogels. (B) The quantification data analysis of relative bone mass volume and Tb.Th in defects sites after it underwent 8 weeks of regeneration with hydrogels. * indicates a significant difference ($P < 0.05$) when compared to CS0. (D, defect site; BV/TV, bone volume fraction; Tb.Th, trabecular thickness; ctl, control).

extent after 4 weeks of implantation as compared to Ctl. Hydrogels might act as a bridge for bone regeneration and play a critical role in bone regeneration with the interaction with native bones.[30,31]

Bone regeneration was further evaluated under histological analysis, as shown in Fig. 12. HE, MT, and VK staining showed increased bone regeneration and new bone formation in the defects filled with CS10 hydrogels compared to Ctl and CS0. After 4 weeks of implantation, some new bone formation was observed in the defects filled by CS0 compared to Ctl, which had minimal bone formation.

Discussion

We have demonstrated thatγ-PGA-GMA was successfully incorporated without affecting the original structural properties of γ-PGA, exhibiting CH and methacryloyl groups at 5.20 and 5.45 ppm, which corresponds to the presence of GMA and the chemical shift that it brought along.[32] In addition, the DS of γ-PGA-GMA was calculated to be 11.28% by comparing the integrated area of vinyl (5.64—6.27 ppm) and 4.13—4.52 ppm (γ-PGA, α-proton).[33]

The FTIR analysis was carried out in the wavelength range of 500 cm^{-1} to 4000 cm^{-1}, where a characteristic absorption band of CS (Si-O-Si) was in the 1150 cm^{-1} region in the CS2, CS5, and CS10 groups, indicating the successful incorporation of CS into hydrogels.[34] Furthermore, it could be noted that the intensities of the CS absorption band increase in line with the concentrations of CS added. Furthermore, —OH groups at 3350 cm^{-1} appeared to decrease with an increase in concentrations of CS, indicating that γ-PGA-GMA hydrogels could be modified with varying concentrations of CS for different requirements and situations. In addition, the CS hydrogels exhibited decreased intensities of C-O-C, -COOC-, and -COOH peaks in 1550 cm^{-1} and 1650 cm^{-1} regions, which correspond to the presence of γ-PGA-GMA.[35]

CS0 had the typical crystalline peaks of γ-PGA at 2θ of 23.2°, 29.6°, and 32.5°., which were noted to increase in line with CS concentrations gradually.[5] The relation of the mechanical properties between CS0 and CS10 was consistent with results reported by others in confirming that CS modification provided enhanced mechanical properties to hydrogels.[36] The result showed these diversities in surface structures were especially evident in groups with higher concentrations of CS, whereby the presence of dense, reticular network structures with micro-level pores could be significantly observed.[37] Previous studies had demonstrated a favorability of micro-environments with roughness, interconnecting networks, and pores for cellular growth and differentiation.[38] Hence, hydrogels involving higher concentrations of CS, which displayed denser surface architectures, were speculated to be able to promote better osteogenesis and regeneration in comparison to other

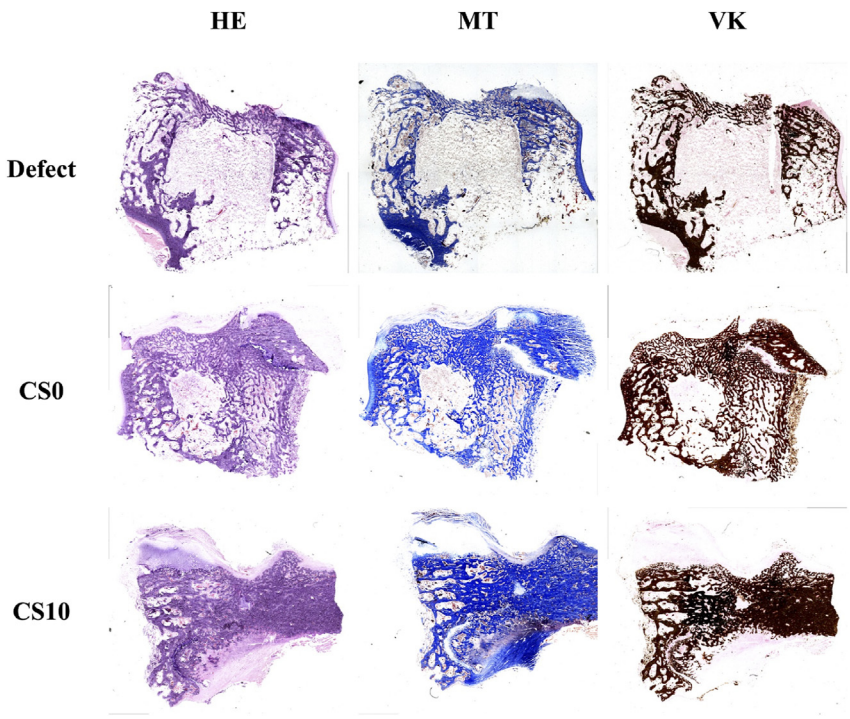

Figure 12 Hematoxylin-eosin (HE), Masson's trichrome (MT), and von Kossa (VK) staining evaluating new bone regeneration quality of CS0 and CS10 hydrogels in a critical-sized bone defect in vivo at 4 and 8 weeks of implantation. The scale bar is 400 μm.

groups.[39] The degradation rates of the CS/γ-PGA-GMA were determined by assessing the pre- and post-immersion weights of the hydrogels. Hard tissues typically take 2 weeks to a month for sufficient regeneration; therefore, CS10 composites were speculated to efficiently support tissue regeneration as the degradation results above indicated.[40]

Shie et al. first reported the potential benefits and roles of Si ions on bone tissue regeneration,[41] which is involved in bone calcification and inhibition of osteoclasts, as they are usually absorbed in the form of meta-silicate. Recent studies have demonstrated that Si ion was involved in regulating proliferation and in the differentiation of stem cells, as well as downstream collagen secretion.[42] Furthermore, it was noted here that the presence of Si ion alone stimulated osteogenesis differentiation of human mesenchymal stem cells in the absence of osteogenic-inducing factors.[5] In addition, the presence of aqueous Si was reported to enhance hydroxyapatite formation on surfaces of hydrogels, which were considered to increase osteoblast secretion of extracellular matrix and strengthen bone-hydrogel integration.[43]

The biocompatibility of the CS/γ-PGA-GMA hydrogels was as expected based on individual biomaterials published by others. γ-PGA was demonstrated to support stem cell proliferation and differentiation, and γ-PGA-GMA induced chondrogenic and osteogenic differentiation of stem cells. On the other hand, CS was also widely reported to be biocompatible for various types of cells, which was also shown to release Si ions that were proven to provide osteogenic, angiogenic, and anti-bacterial capabilities. Several osteogenesis-related markers were evaluated to compare and analyze the effects of CS concentrations in promoting bone regeneration. ALP is a strong booster of bone regeneration as well as a marker of the early stage of bone mineralization. These bone-related markers indicated the positive effects of the CS incorporation on bone regeneration, which showed a direct proportion to CS concentrations in the hydrogels. On the other hand, OC is another early-stage marker of bone turnover and a critical modulator of bone resorption and formations. In addition, both ALP and OC are also considered to integrate existing bones with newly regenerated bone tissues. Therefore, the results collected were consistent with previous studies, indicating that better growth of HUMSC can be achieved with greater concentrations of CS benefitting from its osteoinductive properties, as evidenced by the expression of ALP and OC in the CS10 group.

Bone mineralization was also evaluated using Alizarin Red S staining. The results illustrated the capability of our CS/γ-PGA-GMA hydrogels to provide an excellent microenvironment for bone mineralization and subsequent bone regeneration. CS was reported to release calcium ions and silicate ions, which are inductive for osteogenesis and angiogenesis.[44] In addition, CS-related biomaterials, possessing the alkalinization properties of CS, were argued to have a certain degree of anti-bacterial capabilities.[45] And incorporating γ-PGA-GMA hydrogels enabled us to fabricate hydrogels of various shapes and sizes and yet have osteogenic capabilities and enhanced mechanical properties provided by the addition of CS.

To use the femur defects of the rabbit model further to assess the in vivo osteogenesis of the prepared CS/γ-PGA-GMA. The results of Tb.Th measurements reporting the highest trabecular thickness observed in CS10 were consistent with the findings above. The differences between the results of CS10 and Ctl were demonstrated to be

statistically significant ($P < 0.05$). Therefore, the results robustly suggest that the presence of hydrogels was capable of promoting bone regeneration and that our novel hydrogels, with the addition of CS were able to modify bone regeneration and bone thickness to a large extent after 4 weeks of implantation as compared to Ctl. Hydrogels might act as a bridge for bone regeneration and play a critical role in bone regeneration with the interaction with native bones.[30,31] The histological analysis showed most of the CS10 hydrogels had been degraded and filled with new bone growth. Therefore, the addition of CS elicited more bone regeneration and formation.[43,46,47]

In this study, CS/γ-PGA-GMA hydrogels were successfully fabricated in uniform distribution by DLP processing. Benefitting from the calcium silicate and photo-crosslinker, the mechanical properties of the CS/γ-PGA-GMA hydrogel were increased 5-fold better than those of the γ-PGA-GMA hydrogel. The hydrogels maintained homogeneous morphology and uniform porous structures even with high concentrations of CS. The CS/γ-PGA-GMA hydrogel can elude the disadvantage of rapid degradation, with weight loss reduced to 26% within one month. At the same time, the addition of CS enables the gradual release of Ca and Si ions into the surrounding liquid to promote and enhance cellular activities. Cellular behavior studies demonstrated that CS/γ-PGA-GMA hydrogel stimulated proliferation, differentiation, and Ca mineral deposition of HUMSC in comparison to the γ-PGA-GMA group. Based on the in vivo rabbit femur model, the analysis indicated that the CS/γ-PGA-GMA hydrogel enhanced bone regeneration, appearing at increased levels. These results strongly indicated the crucial advantage of combining different biomaterials in fabricating a promising all-rounded hydrogel for bone regeneration. We hoped this study could be provided to develop high-potential biomaterials for bone tissue regeneration.

Declaration of competing interest

The authors have no conflicts of interest relevant to this article.

Acknowledgments

The authors acknowledge receipt of a grant from the Ministry of Science and Technology (MOST 109-2221-E-039-001-MY3 and 110-2314-B-002-287) of Taiwan, and China Medical University Hospital grants (DMR-110-058) of Taiwan. Experiments and data analysis were performed in part through the use of the Medical Research Core Facilities, Office of Research & Development at China Medical University, Taichung, Taiwan.

References

1. Wu X, Huo Y, Ci Z, et al. Biomimetic porous hydrogel scaffolds enabled vascular ingrowth and osteogenic differentiation for vascularized tissue-engineered bone regeneration. *Appl Mater Today* 2022;27:101478.
2. Sun Y, Li Y, Zhang Y, Wang T, Lin K, Liu J. A polydopamine-assisted strontium-substituted apatite coating for titanium promotes osteogenesis and angiogenesis via FAK/MAPK and PI3K/AKT signaling pathways. *Biomater Adv* 2021;131:112482.
3. Huang Y, Wu C, Zhang X, Chang J, Dai K. Regulation of immune response by bioactive ions released from silicate bioceramics for bone regeneration. *Acta Biomater* 2018;66:81—92.
4. Geng Z, Wu P, Pan H, et al. Robust layer interface in cement additive manufacturing via silicate penetration and precipitation. *Mater Des* 2022;214:110380.
5. Lin YH, Lee KX, Ho CC, Fang MJ, Kuo TY, Shie MY. The effects of a 3D-printed magnesium-/strontium-doped calcium silicate scaffold on regulation of bone regeneration via dual-stimulation of the AKT and WNT signaling pathways. *Biomater Adv* 2022;135:112660.
6. Zhang H, Ma W, Ma H, Qin C, Chen J, Wu C. Spindle-like zinc silicate nano-particles accelerating innervated and vascularized skin burn wound healing. *Adv Healthcare Mater* 2022;11:2102359.
7. Latifi SM, Fathi M, Sharifnabi A, Varshosaz J. In vitro characterisation of a sol—gel derived in situ silica-coated silicate and carbonate co-doped hydroxyapatite nanopowder for bone grafting. *Mater Sci Eng C* 2017;75:272—8.
8. Zheng X, Chen F, Zhang J, Cai K. Silica-assisted incorporation of polydopamine into the framework of porous nanocarriers by a facile one-pot synthesis. *J Mater Chem B* 2016;4:2435—43.
9. Gaihre B, Liu X, Li L, et al. Bifunctional hydrogel for potential vascularized bone tissue regeneration. *Mater Sci Eng C* 2021;124:112075.
10. Sartore L, Manferdini C, Saleh Y, et al. Polysaccharides on gelatin-based hydrogels differently affect chondrogenic differentiation of human mesenchymal stromal cells. *Mater Sci Eng C* 2021;126:112175.
11. Zafeiris K, Brasinika D, Karatza A, Charitidis CA, et al. Additive manufacturing of hydroxyapatite—chitosan—genipin composite scaffolds for bone tissue engineering applications. *Mater Sci Eng C* 2021;119:111639.
12. Kim D, Lee J, Kim G. Biomimetic gelatin/HA biocomposites with effective elastic properties and 3D-structural flexibility using a 3D-printing process. *Addit Manuf* 2020;36:101616.
13. Zhang X, Zhu Y, Cao L, et al. Alginate-aker injectable composite hydrogels promoted irregular bone regeneration through stem cell recruitment and osteogenic differentiation. *J Mater Chem B* 2018;6:1951—64.
14. Wu YHA, Chiu YC, Lin YH, Ho CC, Shie MY, Chen YW. 3D-printed bioactive calcium silicate/poly-ε-caprolactone bioscaffolds modified with biomimetic extracellular matrices for bone regeneration. *Int J Mol Sci* 2019;20:942.
15. Song J, Chen Z, Liu Z, et al. Controllable release of vascular endothelial growth factor (VEGF) by wheel spinning alginate/silk fibroin fibers for wound healing. *Mater Des* 2021;212:110231.
16. Puertas-Bartolomé M, Włodarczyk-Biegun MK, del Campo A, Vázquez-Lasa B, Román JS. Development of bioactive catechol functionalized nano-particles applicable for 3D bioprinting. *Mater Sci Eng C* 2021;131:112515.
17. Su Z, Han C, Liu E, Zhang F, Liu B, Meng X. Formation, characterization and application of arginine-modified chitosan/γ-poly glutamic acid nano-particles as carrier for curcumin. *Int J Biol Macromol* 2021;168:215—22.
18. Liu S, Pu Y, Yang R, et al. Boron-assisted dual-crosslinked poly (γ-glutamic acid) hydrogels with high toughness for cartilage regeneration. *Int J Biol Macromol* 2020;153:158—68.
19. Li L, Liu X, Gaihre B, Li Y, Lu L. Mesenchymal stem cell spheroids incorporated with collagen and black phosphorus promote osteogenesis of biodegradable hydrogels. *Mater Sci Eng C* 2021;121:111812.
20. Fang Y, Guo Y, Ji M, et al. 3D printing of cell-laden microgel-based biphasic bioink with heterogeneous microenvironment for biomedical applications. *Adv Funct Mater* 2022;32:2109810.

21. Borandeh S, van Bochove B, Teotia A, Seppälä J. Polymeric drug delivery systems by additive manufacturing. *Adv Drug Deliv Rev* 2021;173:349—73.
22. Lee AKX, Lin YH, Tsai CH, Chang WT, Lin TL, Shie MY. Digital light processing bioprinted human chondrocyte-laden poly (γ-glutamic acid)/hyaluronic acid bio-ink towards cartilage tissue engineering. *Biomedicines* 2021;9:714.
23. Cao Y, Cheng P, Sang S, et al. 3D printed PCL/GelMA biphasic scaffold boosts cartilage regeneration using co-culture of mesenchymal stem cells and chondrocytes: in vivo study. *Mater Des* 2021;210:110065.
24. Kim W, Kim G. 3D bioprinting of functional cell-laden bioinks and its application for cell-alignment and maturation. *Appl Mater Today* 2020;19:100588.
25. Song S, Liu X, Huang J, Zhang Z. Neural stem cell-laden 3D bioprinting of polyphenol-doped electroconductive hydrogel scaffolds for enhanced neuronal differentiation. *Biomater Adv* 2022;133:112639.
26. Dong Y, Zhang M, Han D, et al. A high-performance GelMA—GelMA homogeneous double-network hydrogel assisted by 3D printing. *J Mater Chem B* 2022;10:3906—15.
27. Hou X, Chen Y, Chen F, et al. The hydroxyapatite microtubes enhanced GelMA hydrogel scaffold with inner "pipeline framework" structure for bone tissue regeneration. *Composites Part B* 2022;228:109396.
28. Su CC, Kao CT, Hung CJ, Chen YJ, Huang TH, Shie MY. Regulation of physicochemical properties, osteogenesis activity, and fibroblast growth factor-2 release ability of β-tricalcium phosphate for bone cement by calcium silicate. *Mater Sci Eng C* 2014;37:156—63.
29. Shie MY, Chen DCH, Wang CY, Chiang TY, Ding SJ. Immersion behavior of gelatin-containing calcium phosphate cement. *Acta Biomater* 2008;4:646—55.
30. Pu X, Tong L, Wang X, et al. Bioinspired hydrogel anchoring 3DP GelMA/HAp scaffolds accelerates bone reconstruction. *ACS Appl Mater Interfaces* 2022;14:20591—602.
31. Li Z, Zhao Y, Wang Z, et al. Engineering multifunctional hydrogel-integrated 3D printed bioactive prosthetic interfaces for osteoporotic osseointegration. *Adv Healthcare Mater* 2022;11:2102535.
32. Sk MM, Das P, Panwar A, Tan LP. Synthesis and characterization of site selective photo-crosslinkable glycidyl methacrylate functionalized gelatin-based 3D hydrogel scaffold for liver tissue engineering. *Mater Sci Eng C* 2021;123:111694.
33. Später T, Mariyanats AO, Syachina MA, et al. In vitro and in vivo analysis of adhesive, anti-inflammatory, and proangiogenic properties of novel 3D printed hyaluronic acid glycidyl methacrylate hydrogel scaffolds for tissue engineering. *ACS Biomater Sci Eng* 2020;6:5744—57.
34. Dong Y, Chen H, Qiao P, Liu Z. Development and properties of fish gelatin/oxidized starch double network film catalyzed by thermal treatment and schiff' base reaction. *Polymers* 2019;11:2065.
35. Sun A, He X, Li L, et al. An injectable photopolymerized hydrogel with antimicrobial and biocompatible properties for infected skin regeneration. *NPG Asia Mater* 2020;12:25.
36. Ma H, Yu Q, Qu Y, Zhu Y, Wu C. Manganese silicate nanospheres-incorporated hydrogels: starvation therapy and tissue regeneration. *Bioact Mater* 2021;6:4558—67.
37. Gao L, Zhou Y, Peng J, et al. A novel dual-adhesive and bioactive hydrogel activated by bioglass for wound healing. *NPG Asia Mater* 2019;11:66.
38. Siebert L, Luna-Cerón E, García-Rivera LE, et al. Light-controlled growth factors release on tetrapodal ZnO-incorporated 3D-printed hydrogels for developing smart wound scaffold. Light-controlled growth factors release on tetrapodal ZnO-incorporated 3D-printed hydrogels for developing smart wound scaffold. *Adv Funct Mater* 2021;31:2007555.
39. Zheng A, Cao L, Liu Y, et al. Biocompatible silk/calcium silicate/sodium alginate composite scaffolds for bone tissue engineering. *Carbohydr Polym* 2018;199:244—55.
40. Qiu J, Ahn J, Qin D, Thomopoulos S, Xia Y. Biomimetic scaffolds with a mineral gradient and funnel-shaped channels for spatially controllable osteogenesis. *Adv Healthcare Mater* 2022;11:2100828.
41. Shie MY, Ding SJ, Chang HC. The role of silicon in osteoblast-like cell proliferation and apoptosis. *Acta Biomater* 2011;7:2604—14.
42. Yu Q, Chang J, Wu C. Silicate bioceramics: from soft tissue regeneration to tumor therapy. *J Mater Chem B* 2019;7:5449—60.
43. Kao CT, Chiu YC, Lee AKX, et al. The synergistic effects of Xu Duan combined Sr-contained calcium silicate/poly-ε-caprolactone scaffolds for the promotion of osteogenesis marker expression and the induction of bone regeneration in osteoporosis. *Mater Sci Eng C* 2021;119:111629.
44. Li K, Lu X, Razanau I, et al. The enhanced angiogenic responses to ionic dissolution products from a boron-incorporated calcium silicate coating. *Mater Sci Eng C* 2019;101:513—20.
45. Chen YW, Shen YF, Ho CC, et al. Osteogenic and angiogenic potentials of the cell-laden hydrogel/mussel-inspired calcium silicate complex hierarchical porous scaffold fabricated by 3D bioprinting. *Mater Sci Eng C* 2018;91:679—87.
46. Liu L, Yu F, Li L, et al. Bone marrow stromal cells stimulated by strontium-substituted calcium silicate ceramics: release of exosomal miR-146a regulates osteogenesis and angiogenesis. *Acta Biomater* 2021;119:444—57.
47. Zhou P, Xia D, Ni Z, et al. Calcium silicate bioactive ceramics induce osteogenesis through oncostatin M. *Bioact Mater* 2021;6:810—22.